ELSEVIER

Journal of Power Sources 83 (1999) 32–40

JOURNAL OF POWER SOURCES

www.elsevier.com/locate/jpowsour

Corrosion behaviour of sensitized AISI-type 316L stainless steel in molten carbonate fuel cell in cathode-gas environment

Kab Soo Lee [a], Kyehyun Cho [b,1], Tae Hoon Lim [b,*], Seong-Ahn Hong [b], Hwayong Kim [a]

[a] *Division of Chemical Engineering, Seoul National University, Seoul, South Korea*

[b] *Battery and Fuel Cell Research Center, Korea Institute of Science and Technology, 39-1, Hawolkog-dong, Sungbuk-ku, Seoul, 136-791, South Korea*

Received 27 January 1999; accepted 23 February 1999

Abstract

Corrosion of the cell components is a major problem in the development of the molten carbonate fuel cell (MCFC). This study describes the effect of sensitization on the corrosion characteristics of AISI-type 316L stainless steel in a 62/38 lithium–potassium carbonate eutectic melt in the cathode-gas environment. After solution treatment at 1200°C for 4 h followed by sensitization treatment at 650°C for predetermined time, the corrosion behaviour of the sensitized sample is analyzed electrochemically by a potentiodynamic method. The sensitized sample displays behaviour which is typical of active–passive transition. Increasing the time of the sensitization treatment causes the corrosion potential to shift in the cathodic direction. In addition, the passive film becomes more unstable and supports a high passive current, i.e., the substrate is more susceptible to intergranular corrosion (IGC). Morphological observation of samples immersed in a carbonate melt reveal a change in corrosion mechanism from initial IGC to localized corrosion. Huge cavities develop from grooves after 200 h of immersion in a carbonate melt. A combination of a Cr-depleted region due to sensitization and decreasing oxygen concentration from top to bottom of the oxide layer, is considered to be the main reason for the change in corrosion morphology.

Keywords: Molten carbonate fuel cell; Sensitization; Stainless steel; Intergranular corrosion; Cathode-gas environment

1. Introduction

The molten carbonate fuel cell (MCFC), a so-called second generation fuel cell, is an energy conversion device with high efficiency and low atmospheric emissions. To be economically competitive in the market, however, an MCFC must be able to maintain its performance over a lifetime of 40,000 h. Up to now, no MCFC regardless of its size has successfully demonstrated such an ability. Several life-limiting factors, such as electrolyte loss, NiO dissolution and degradation of separator material due to corrosion, have been recognized. Among these, the problem of corrosion of the separator appears to be the most crucial in both technical and economical respects. Corrosion in MCFC, i.e., harmful reactions between the separator material and the carbonate melt, results not only in the loss of separator function but also in the loss of electrolyte, and eventually leads to increase in internal resistance and gas crossover. Accordingly, high-cost material, for example austenitic stainless steel is required, and this, to some extent, prevents MCFCs from becoming commercialized [1].

Following a general discussion on the corrosion of separators in MCFCs by Donado et al. [2], various studies with chromium [3,4], nickel [5], stainless steels [6], nickel-based alloys [7] and nickel–iron alloys [8] were performed in either a MCFC gas atmosphere or a carbonate melt in order to understand the corrosion process and to select the best material for separators. The results of studies [4,7,8] obtained by quasi-stationary polarization curve measurements and cyclic voltammetry, clearly indicated the important effect of electrochemical pretreatment on passive film formation which determines the initial rate of corrosion, as well as the beneficial effect of chromium or aluminium

* Corresponding author. Tel.: +82-2-958-5273; Fax: +82-2-958-5199; E-mail: thlim@kistmail.kist.re.kr

[1] Current address: School of Metallurgy and Materials, Yeungnam University, Kyungsan, South Korea.

0378-7753/99/$ - see front matter
PII: S0378-7753(99)00245-1

addition to the matrix on corrosion resistance of stainless steels and nickel-based alloys. In a corrosion experiment with stainless steels in carbonate melt and an anode-gas environment, a dual-layered oxide structure, which comprised a iron–lithium-oxide surface layer followed by an inner layer rich in Cr_2O_3, was observed [6,9,10]. It was also found that the metal beneath the oxide layer was enriched in nickel and depleted in chromium. Severe carburization of the alloy near the surface and sensitization of the bulk alloy were also commonly observed. As Shores and Pischke [11] pointed out, however, the interpretation of these results must be very comprehensive because the real corrosion environment in MCFC operating conditions is too complicated to be represented by a model experiment. Hence, a basic metallurgical aspect like the sensitization effect should be taken into account to evaluate a separator material such as AISI-type 316L stainless steel.

It is well-known that austenitic stainless steels can suffer intergranular corrosion (IGC) due to sensitization. When heated in the range of 425 to 815°C, carbon and chromium in stainless steel diffuse to the grain boundaries to form Cr-rich $M_{23}C_6$ carbide and leave a Cr-depleted region nearby. This latter region becomes more susceptible to corrosion than the rest of grain area. At 650°C, the usual MCFC operating temperature, a separator made with austenitic stainless steel is readily sensitized to be attacked by IGC [12,13]. According to the sensitization diagram [14], heating at 650°C for only 1 h can result in the sensitization of stainless steel in which the carbon content is as low as 0.03 wt.%. To avoid such a catastrophic degradation, several methods can be adopted: (i) heat treatment at a higher temperature; (ii) increased chromium content in matrix; (iii) decreased carbon content to below 0.03 wt.%; (iv) addition of strong carbide former. Neither heat treatment at higher temperature nor increase in chromium content can be applied because of technical and economical constraints. Hence, AISI-type 316L stainless steel seems to be the most appropriate choice since its very low 'C' content is expected to render it relatively free from sensitization. In aqueous media, AISI-type 316L stainless steel shows excellent resistance to IGC [15–17]. Nevertheless, IGC attack on AISI-type 316L stainless steel in MCFC operating conditions has been reported [10,18].

This study examines the effect of sensitization on the corrosion characteristics of AISI-type 316L stainless steel in 62/38 lithium–potassium carbonate eutectic melt at 650°C. Electrochemical measurement (by a potentiodynamic method) and morphological observation of samples immersed in carbonate melt are adopted as experimental methods.

Table 1
Bulk composition of AISI-type 316L stainless steel

Element	C	Cr	Ni	Mo	Mn	Si	P	S	Fe
Composition (wt.%)	0.03	16–18	10–14	2.0–3.0	2.0	1.0	0.014	0.03	bal.

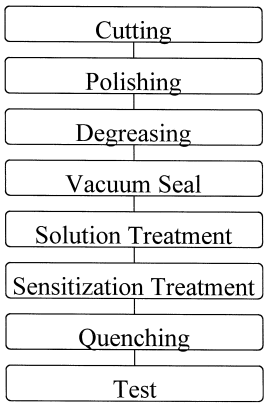

Fig. 1. Flow diagram of sample treatment.

2. Experimental

The bulk composition of AISI-type 316L stainless steel is given in Table 1.

The procedure used for sample preparation is depicted in Fig. 1. All samples had dimensions of $2 \times 2 \times 0.1$ cm and were washed in distilled water followed by ultrasonic degreasing in acetone. To obtain a mirror-like surface, they were polished with 240 grit sand paper and 0.05 μm

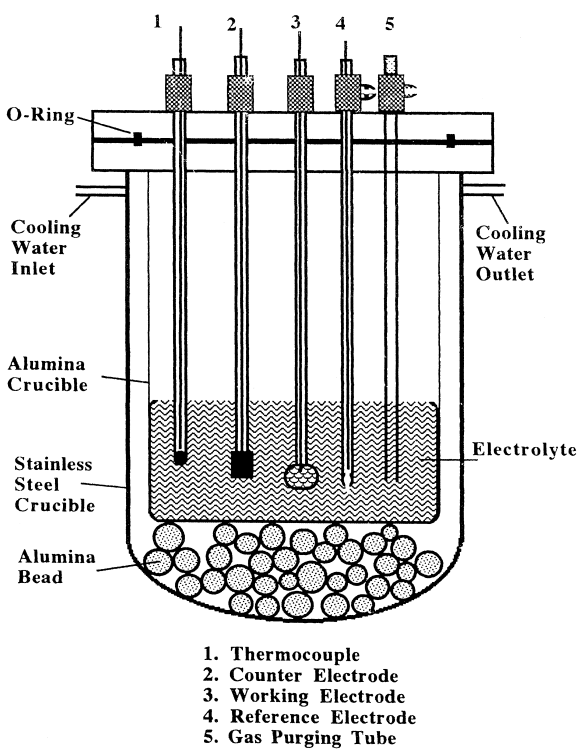

Fig. 2. Schematic diagram of pot-cell system.

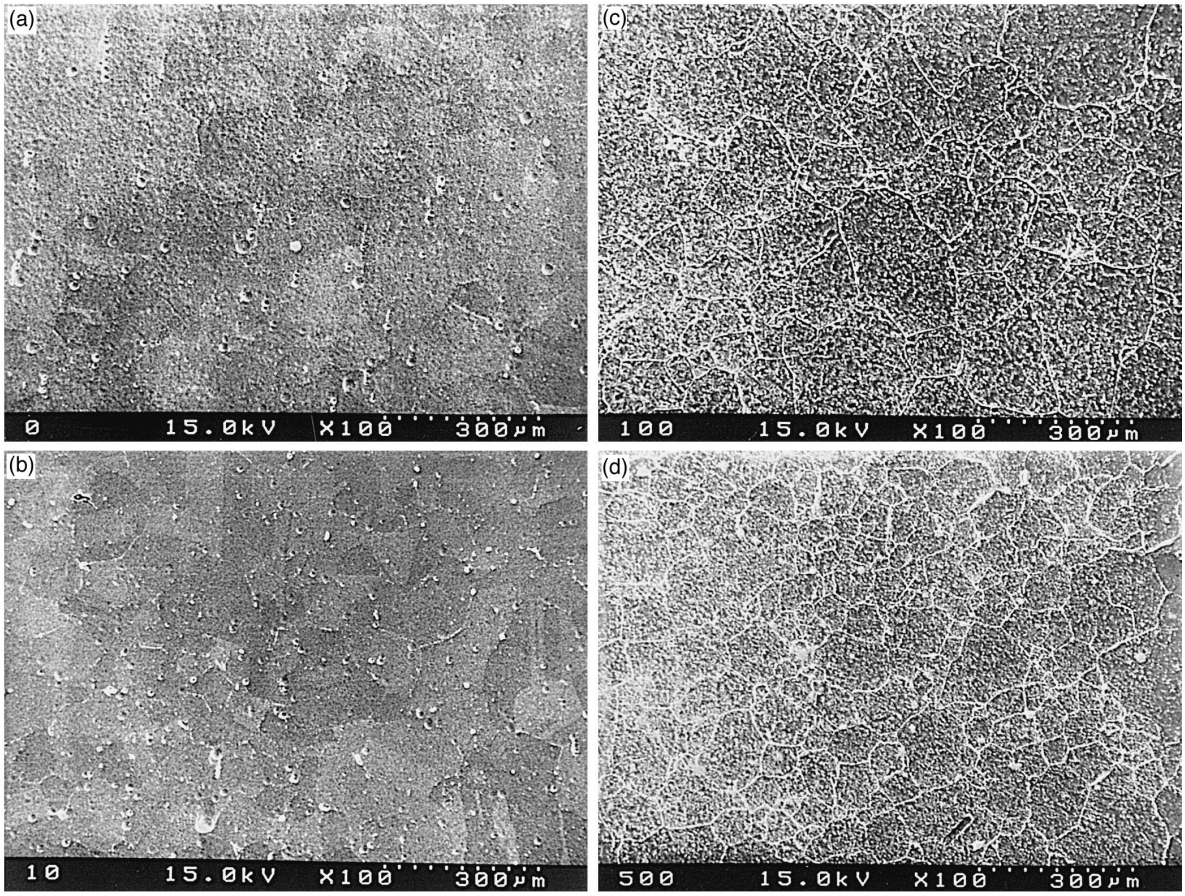

Fig. 3. Surface images of samples after etching in saturated KCl solution. Sensitization treatment: (a) none; (b) 10 h; (c) 100 h; (d) 500 h.

alumina powder. After vacuum sealing in quartz tubes, the samples were subjected to solution treatment at 1200°C for 4 h, followed by cooling down to 650°C and ageing for a predetermined time (10, 100, 500 h) for the sensitization treatment. An ice-water quenching process was adopted to avoid any undesired change in the sample at the final stage of the heat-treatment schedule.

To verify the effect of the sensitization treatment, an etching process was executed in saturated KCl solution. An etching current of 1 A cm^{-2} was applied for 5 min to each sensitized sample in order to dissolve the chromium carbide formed in the grain boundaries during the sensitization treatment. The surface morphology of the sample was then observed with scanning electron microscopy (SEM).

Electrochemical tests were performed in a typical pot-cell system, as shown in Fig. 2. The reference electrode and the counter electrode were made from a gold wire and a gold flag, respectively. A sensitized or non-sensitized sample was used as the working electrode, which was spot-welded with gold wire. The reference gas was a mixture of 33% oxygen and 67% carbon dioxide. This gas mixture was bubbled through an alumina tube in the carbonate melt. The composition of the cathode atmosphere gas mixture was the same as the reference gas mixture, and the flow rate was 200 cc/min. For an anode gas atmosphere, a hydrogen and carbon dioxide mixture (80:20) was supplied at a flow rate of 200 cc/min. A well dried 62/38 (mole ratio) lithium and potassium carbonate mixture was put into a pure alumina crucible placed in an electric furnace.

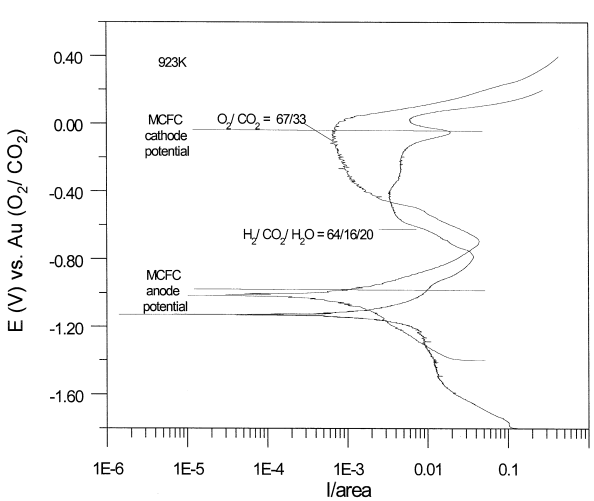

Fig. 4. Polarization curve of non-sensitized AISI-type 316L stainless steel in Li/K carbonate eutectic melt at 650°C. (Scan rate = 0.1 mV s^{-1}).

The electrochemical experiments were performed when the temperature of the carbonate melt reached 650°C. The potentiodynamic method was applied at a scan rate of 0.1 mV s^{-1} in the potential range −1400 to 400 mV. The measurements were recorded with an EG and G potentiostat/galvanostat Model 273A which was controlled by a computer running M352 corrosion software.

Immersion tests were also carried out in the same pot-cell. After the immersion tests, the samples were removed from the carbonate melt and washed by an ultrasonic cleaner with distilled water. The surface morphology of each sample was observed with an optical microscope and a SEM. In the vicinity of IGC due to sensitization, cross-section compositional analysis was accomplished by an electron probe microanalyzer (EPMA).

3. Results and discussion

The surface images of sensitized samples and non-sensitized stainless steel after etching in saturated KCl solution are illustrated in Fig. 3. This etching technique is used not to dissolve the Cr-depleted areas near the grain boundaries, but to dissolve the chromium carbide formed in the grain boundaries during the sensitization treatment. Thus, the existence of the dissolved grain boundaries shown in Fig. 3 implies that chromium carbide has actually been formed during the sensitization treatment, otherwise the surface would remain clean. Moreover, Fig. 3 shows clearly that the degree of sensitization depends strongly on the time of sensitization. While a sample surface without sensitization treatment remains clean after the etching test, but the grain boundaries of the sensitized samples become more visible with increasing the period of sensitization. The grain size is about 30 μm, which is the typical grain size of the stainless steel.

Fig. 4 shows polarization curves for samples without sensitization treatment, obtained in either an anode or a cathode inlet gas atmosphere, in a carbonate melt at 650°C. In the cathode gas atmosphere, the polarization curve includes four typical regions: cathodic, active, passive and transpassive regions, and the corrosion potential is about −1020 mV. Around this corrosion potential, the measured potential-current density curves display linear segments in

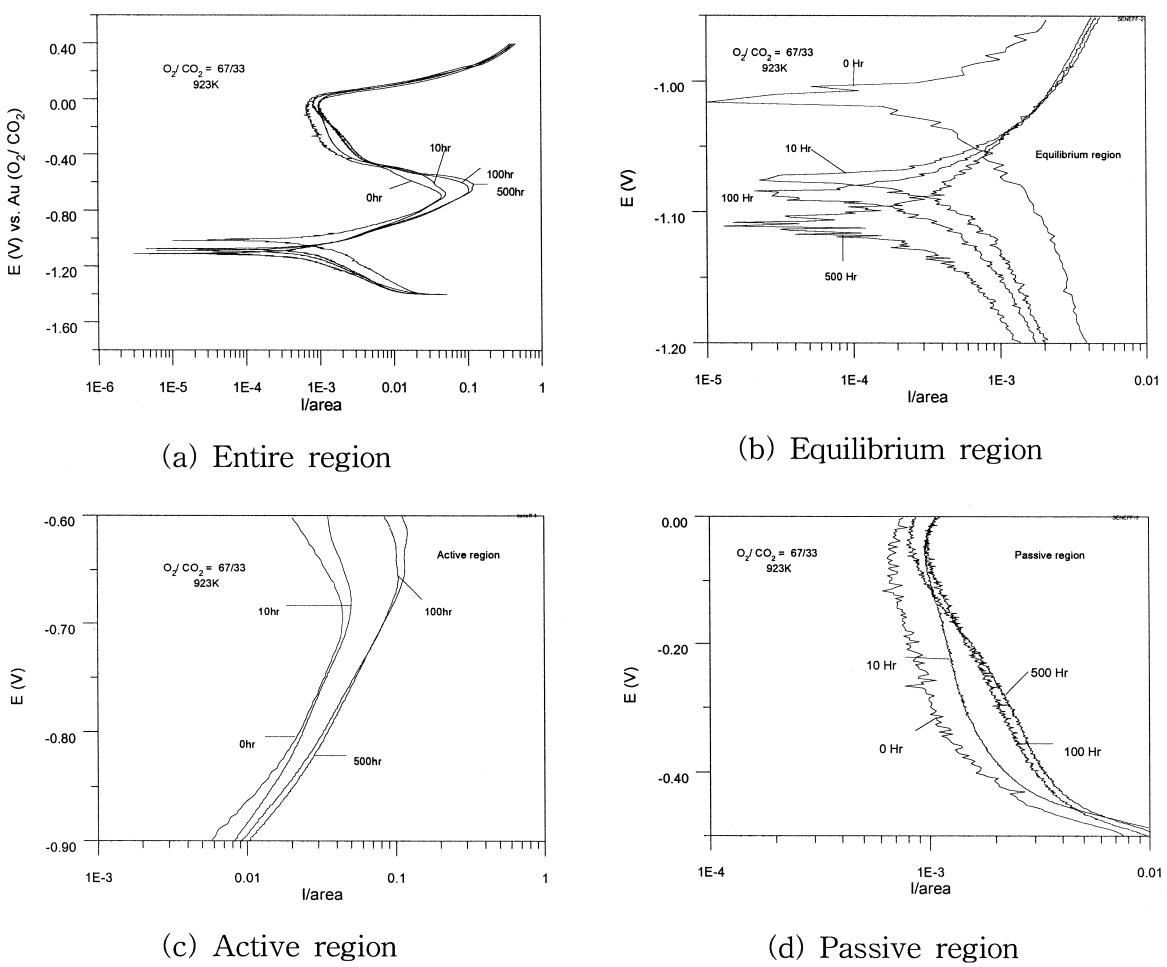

Fig. 5. Polarization curve of AISI-type 316L stainless steel in Li/K carbonate eutectic melt at 650°C. (Scan rate = 0.1 mV s^{-1}.): (a) entire region; (b) equilibrium region; (c) active region; (d) passive region.

both the negative and positive directions. These segments are usually referred to as Tafel regions. At a potential of about −100 mV, the so-called primary passivation potential, an anodic peak current exists. Above this potential, passivation begins. The passive region exists over a wide range of potential, i.e., the corrosion rate is very low. The transpassive region begins around 0 mV, where the current sharply increases. By contrast, the corrosion potential in the anode gas atmosphere shifts in the positive direction by about 100 mV. A large difference in behaviour is found between the two gas atmospheres in the passive region where the current measured in the cathode gas atmosphere has a much lower value. This is because the stability of the passive film depends strongly on the oxygen concentration.

Corrosion takes place only when the actual electrode potential is more positive than the corrosion potential of the anodic reaction. Theoretically, the corrosion rate depends proportionally on the driving force expressed as the electrode potential. Thus, as the actual electrode potential becomes more positive, the corrosion proceeds at a faster rate. Most transition metals, however, have the ability to passivate by forming a protective oxide layer which, in turn, produces a passivation state even at more positive potentials than the corrosion potential, as shown in Fig. 4.

Corrosion reactions in a MCFC environment can be represented for a given metal M by the following equations [2–5]:

$$M \leftrightarrow M^{2+} + 2e^- \quad (1)$$

$$M + O^{2-} \leftrightarrow MO + 2e^- \quad (2)$$

$$M + 2OH^- \leftrightarrow MO + H_2O + 2e^- \quad (3)$$

$$M + CO_3^{2-} \leftrightarrow MO + CO_2 + 2e^- \quad (4)$$

Based on these equations, the corrosion of stainless steel can proceed in two modes. First, a metal, M, can react directly with oxidizing ions in the electrolyte, as expressed in Eqs. (2)–(4), to produce an oxide layer. At a particular electrode potential, this oxide film begins to act as a passivating agent. Chromium oxide is known to be the most stable and protective oxide layer [10,11]. Hence, the chromium content in a stainless steel is very important in determining the degree of passivity. In the second mode of corrosion, the metal may dissolve directly in the electrolyte by Eq. (1). This dissolution reaction may be accelerated when the electrode potential moves towards more positive values.

The above four corrosion reactions can be affected greatly by surroundings. For example, the composition of the gas atmosphere can determine the corrosion phenomenon as a whole by controlling the stability of passive film and the solubility of the metal in the electrolyte. When dealing with corrosion problems in an MCFC, this fact should be taken into consideration. Because the local environment of a MCFC cell frame varies from one location to another, the wet seal area (anode, cathode), gas channel, current-collector, etc., are exposed to different environments. In fact, a post-analysis result, although not included in this paper, revealed [19] a variety of corrosion phenomena in terms of type and severity.

The effect of sensitization treatment time on polarization of AISI-type 316L. stainless steel in cathode gas and in a carbonate melt is shown in Fig. 5(a). In spite of the fact that the sensitization effect is limited only in the vicinity of grain boundaries, the anodic current increases considerably over the entire passive range. For more detailed observation, these polarization curves are divided into three distinctive regions, namely, the equilibrium, active and passive regions (Fig. 5(b) to (d), respectively).

In the equilibrium region, the effect of sensitization treatment time on corrosion potential is remarkable. On increasing the degree of sensitization, the corrosion potential shifts in a positive direction, that is to say thermodynamically to more corrosion-susceptible state. This result is in consistent with a previous result measured in an aqueous electrolyte by Ramamurthy et al. [20].

In the active region, the passive potential shifts slightly in the anodic direction with increase in the sensitization treatment time, and the peak corrosion currents of a sensitized sample treated for 100 and 500 h are about 2.5 times higher than that of the nonsensitized sample. A similar result has been observed by Osozawa et al. [21,22] in aqueous electrolytes and it was concluded that the higher peak current was due to the absence of passive film formation by virtue of depletion of chromium in the grain boundary areas. Because the potential of the anode wet seal area of the MCFC imposed by its environment usually belongs to this region, the corrosion resistance of this area will be significantly reduced by the sensitization which cannot be avoided during MCFC operation. When bare AISI-type 316L stainless steel is used, severe corrosion attack on anode wet seal area is observed [19]. Therefore,

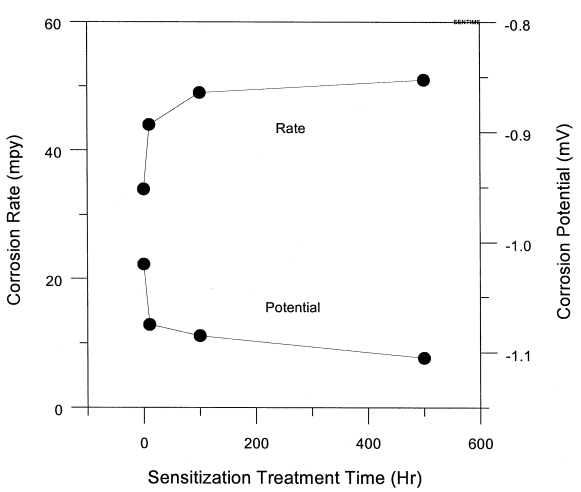

Fig. 6. Effect of sensitization on corrosion rate and potential.

corrosion protection by a proper method such as aluminium coating is indispensable.

In the passive region, the corrosion current tends to increase with increase of the sensitization treatment time. In a microscopic view, the passive state is a steady state between formation and dissolution of the passive oxide layer. Thus, the increased corrosion current due to sensitization means that the stability of the passive film on sensitized stainless steel is not as excellent as that of a filmon non-sensitized steel. The increment in corrosion current in the passive region which the environmental potential of cathode wet seal area belongs to, is not expected to cause such a serious corrosion problem as that observed in the active region. According to corrosion analysis after MCFC operation, the cathode wet seal area made with bare AISI-type 316L stainless steel does not suffer extensively from corrosion attack but undergoes uniform corrosion.

The effect of sensitization treatment time on the corrosion rate and the corrosion potential is shown in Fig. 6. The corrosion rate in the equilibrium region was calculated by the Tafel extrapolation method. With increasing sensitization treatment up to 100 h, the calculated corrosion rate is rapidly increased from 34 to about 50 mpy, but stays at 50 mpy after that. This implies that the sensitization of AISI-type 316L stainless steel is terminated in a short time. A very small amount of carbon content in this stainless steel may be one of the plausible reasons for the early termination of sensitization. Based on this observation, it can be concluded with caution that the direct effect of sensitization on corrosion, for example IGC, would not persist for a long time.

After the potentiodynamic test, the cross-sections of non-sensitized and 100-h sensitized samples were examined by EPMA. The results are shown in Fig. 7. During the potentiodynamic tests, these samples had been immersed in a carbonate melt with a cathode gas atmosphere for only 5 h; nevertheless, both samples have well-developed oxide layers on their surfaces which indicates that very fast corrosions have taken place. The results in Fig. 7 also show that corrosion of the sensitized sample proceeds much faster than that of the non-sensitized counterpart.

An SEM image of the surface of a non-sensitized sample after an immersion test in a carbonate melt at

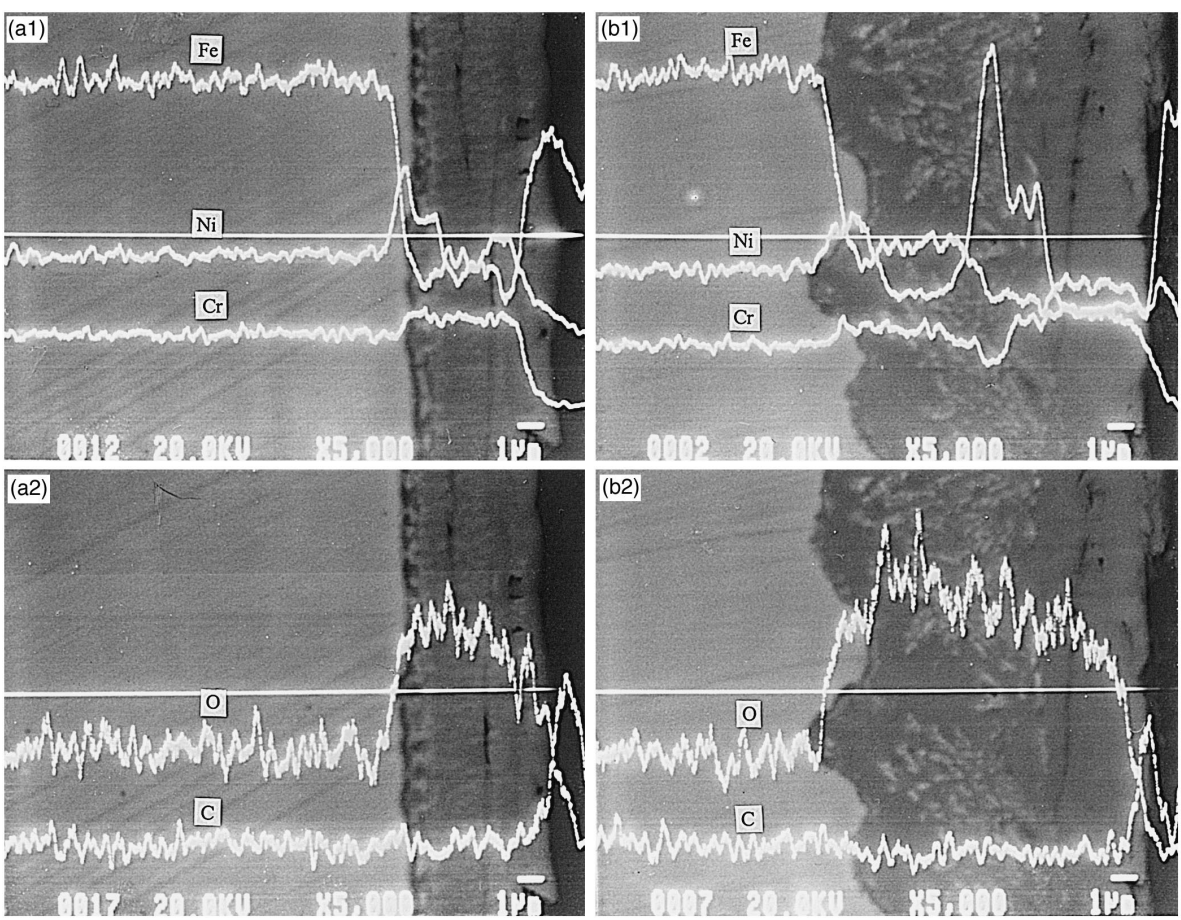

Fig. 7. Concentration profiles of elements in cross-section as analyzed by EPMA after potentiodynamic test: (a) without sensitization; (b) 100 h sensitization.

Fig. 8. Electron micrograph of surface of sample immersed for 200 h: (a) ×1000; (b) ×20,000.

650°C for 200 h is given in Fig. 8. The regions in the vicinity of the grain boundaries are severely attacked and dissolved out to produce deep grooves along the grain boundaries. These might be initiated through chromium depletion by sensitization during the immersion period, as explained in Fig. 3. Some insights on the size as well as the morphology of the grooves are likely to provide a clue for understanding the IGC observed in Fig. 8. The line-like shape of the deep chromium carbide groove of 0.16 μm width strongly suggests that a chromium depletion region by chromium carbide formation is responsible for IGC. This result is closely comparable with other observations obtained in an aqueous electrolyte system [23]. A recent study with a high resolution TEM has revealed an increase in chromium at the grain boundaries due to chromium carbide precipitation to leave a Cr-depleted zone behind. Also, the kinetic model developed by Iyer and Pickering [24] and Bennett and Pickering [25,26] has predicted that the width of the Cr-depleted zone on each side of the grain boundary and the chromium carbide-rich zone is 0.06 and 0.04 μm, respectively. This results in a corrosion-susceptible area of total width 0.16 μm. This agreement between the experimental and the calculated widths is further evidence of the role of Cr-depleted zone in IGC.

The change in the morphology of a corroded area of a sample and its schematic representation with increasing immersion time in a carbonate melt at 650°C are shown in Fig. 9. The schematic corrosion morphology as depicted in Fig. 9(b), (d), (f) and (h) is in a one-to-one correspondence to the electron micrographs in Fig. 9(a), (c), (e) and (g), respectively. The oxide layer on the sample immersed for 10 h is relatively thin and uniform with a thickness of 1.6 μm [19], yet the groove between grains is not clearly visible. By contrast, the thickness of the oxide layer on the sample immersed for 50 h reaches 5.3 μm and the initiation of unexpected corrosion behaviour at the interface between the oxide layer and the matrix can be observed. This interesting phenomenon of metal dissolution propagating from a Cr-depleted grain boundary to the inside of the oxide layer becomes sufficient to cause a change in the corrosion morphology, as shown in Fig. 9(f) and (h), when the immersion time is over 50 h. With increasing depth from the surface, the groove width becomes greater than the expected value. As a consequence, the initial groove turns into a cavity after 100 h of immersion. Fig. 9 clearly shows that the interface, x_{da}, which distinguishes the area under IGC attack from bulk metal dissolution moves towards the surface with increasing immersion time. The location of x_{da} at 50, 100 and 200 h of immersion is 4.7, 3.1 and 2.5 μm below the surface, respectively. These observations imply that the corrosion behaviour of AISI-type 316L stainless steel in a carbonate melt cannot be explained solely by the IGC mechanism, but by a combination of IGC and classical localized corrosion, i.e., so-called 'crevice corrosion' in aqueous media [27], in which the active/passive interface moves upwards towards the opening of the cavity due to local environment changes as the immersion time and the distance from the surface increase. In other words, corrosion begins at the Cr-depleted area to produce grooves along the grain boundaries, but bulk metal dissolution by a crevice corrosion mechanism soon takes over to create a large cavity in the oxide layers. The exceptionally large width and the volume of cavity after 200 h of immersion reaches 35 μm and 4170 μm^3, respectively, calculated on the assumption of a cone shape for the dissolved region, provides further evidence for the proposed combined corrosion mechanism.

The relatively low oxygen concentration at the interface between the oxide layer and the matrix compared with that at the surface is believed to play a responsible role in bulk metal dissolution, just like its role in typical crevice corrosion. Corrosive attack, even on stainless steel, tends to proceed where oxygen activity or concentration is insufficient to make stable passive films. Furthermore, in this particular experiment, carbon dioxide concentration also contributes to the corrosion rate by controlling the basicity of a carbonate melt as well as participating in peroxide ion, O_2^{2-}, formation, as shown in Eq. (5). It is well-known that the solubility of corrosion product depends strongly on the basicity of the carbonate melt and that the peroxide ion

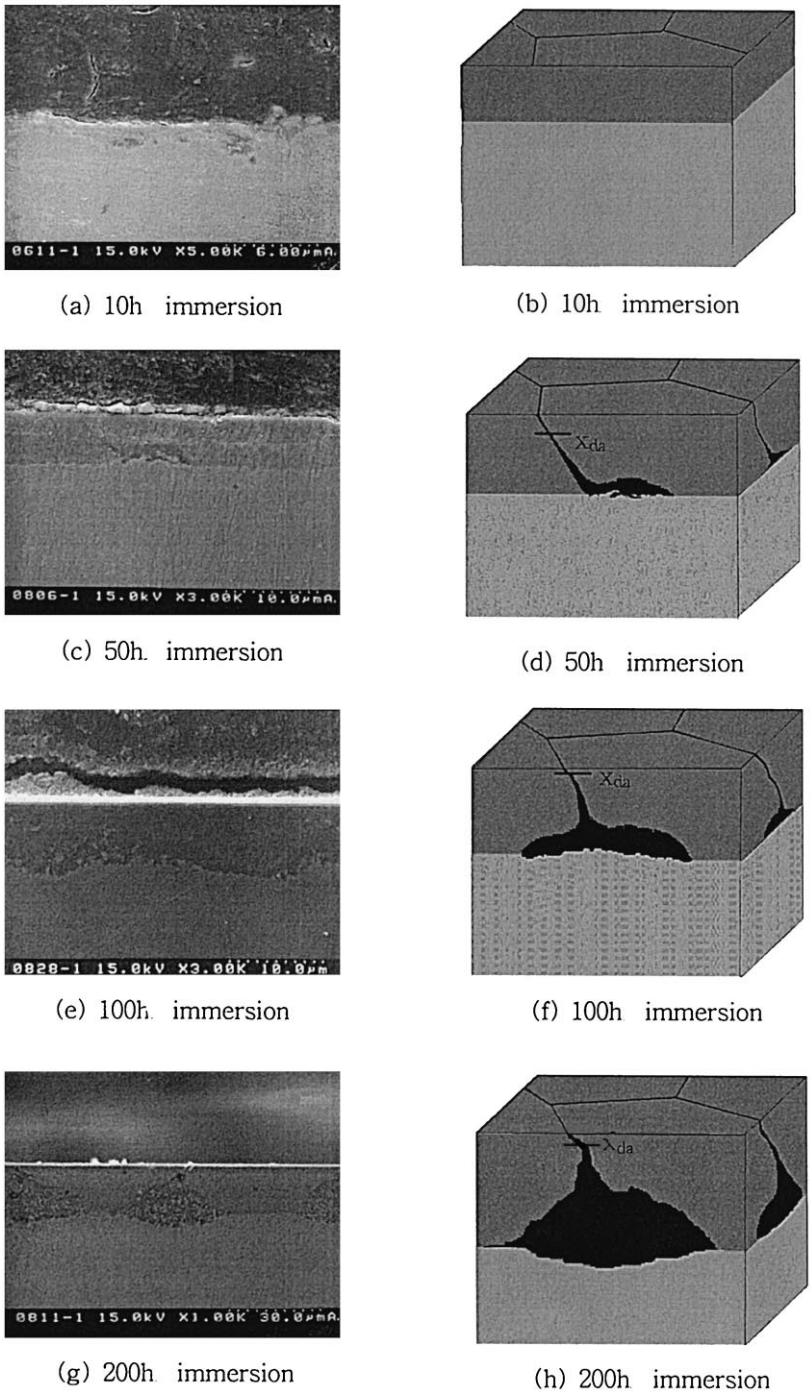

Fig. 9. Electron micrograph of cross-section and schematic drawing of samples with variation of immersion time: (a), (b) 10 h; (c), (d) 50 h; (e), (f) 100 h; (g), (h) 200 h.

content influences the stability of the passive film [28,29].

$$\frac{1}{2}O_2(\text{gas}) + CO_3^{-2} = O_2^{-2} + CO_2(\text{dissolved}) \quad (5)$$

In this work, observations and speculated reasons regarding corrosion on AISI-type 316L in a carbonate melt have been reported. The details of the corrosion mechanism associated with the bulk metal dissolution such as oxygen diffusion through grooves by IGC, peroxide ion concentration profile, etc., have yet to be investigated.

4. Conclusions

The corrosion behaviour of AISI-type 316L stainless steel in an MCFC operating condition has been investi-

gated with particular reference to the effect of sensitization. Polarization curves obtained by an electrochemical potentiodynamic method and SEM observations on sample morphology after immersion in a carbonate melt are combined to understand the corrosion process. The results are summarized as follows.

1. AISI-type 316L stainless steel, with or without sensitization, in either a cathode or an anode gas atmosphere displays typical polarization behaviour and has cathodic, active, passive and transpassive regions. The polarization curve of a sample in an anode gas atmosphere has weaker passivation ability due to higher corrosion current in the passive region.

2. As the sensitization time increases, the corrosion potential shifts in the cathodic direction and the corrosion current becomes higher. The corrosion rate calculated by the Tafel method increases from 34 to 50 mpy after 100 h of sensitization treatment at 650°C.

3. From morphological observation of samples immersed in a carbonate melt, the change in the corrosion process or mechanism from initial IGC due to sensitization to localized corrosion is probably due to the oxygen concentration profile. As a result, large cavities develop from grooves along grain boundaries after 200 h of immersion in a carbonate melt.

References

[1] K. Kinoshita, F.R. McLarnon, E.J. Cairns, Fuel Cells A Hand Book, Lawrence Berkeley Laboratory, California, 1988, p. 64.
[2] R.A. Donado, L.G. Marianowski, H.C. Maru, J.R. Selman, J. Electrochem. Soc. 131 (1984) 2535.
[3] H.S. Hsu, J.H. DeVan, J. Electrochem. Soc. 133 (1986) 2077.
[4] J.P.T. Vossen, R.C. Makkus, J.H.W. de Wit, J. Electrochem. Soc. 143 (1996) 66.
[5] J.P.T. Vossen, L. Plomp, J.H.W. de Wit, J. Electrochem. Soc. 141 (1994) 3040.
[6] D.A. Shores, P. Singh, Proceedings of the Symposium in Molten Carbonate Fuel Cell Technology, in: J.R. Selman, T.D. Claar (Eds.), The Electrochemical Society, Pennington, NJ, 1984, p. 271.
[7] J.P.T. Vossen, L. Plomp, J.H.W. de Wit, G. Rietveld, J. Electrochem. Soc. 142 (1995) 3327.
[8] J.P.T. Vossen, A.H.H. Janssen, J.H.W. de Wit, J. Electrochem. Soc. 143 (1996) 58.
[9] P. Singh, H.C. Maru, Stability of Iron and Nickel Base Alloys in Molten Carbonate Fuel Cell, in Corrosion 85, NACE, Houston, Paper, 1985, p. 344.
[10] C.Y. Yuh, Proceedings of the Symposium in Molten Carbonate Fuel Cell Technology, in: D.A. Shores, J.R. Selman (Eds.), The Electrochemical Society, Pennington, NJ, 1993, p. 368.
[11] D.A. Shores, M.J. Pischke, Proceedings of the Symposium in Molten Carbonate Fuel Cell Technology, in: D.A. Shores, J.R. Selman (Eds.), The Electrochemical Society, Pennington, NJ, 1993, p. 214.
[12] D.A. Jones, Principles and Prevention of Corrosion, 2nd edn., Prentice Hall, New Jersey, 1996, p. 292.
[13] M.G. Fontana, Corrosion Engineering, 3rd edn., McGraw-Hill, New York, 1986, p. 78.
[14] R.M. Davison, T. DeBold, M.J. Johnson, Metals Handbook, Vol. 13, Corrosion, 9th edn., ASM, Metals Park, OH, 1987, p. 547.
[15] R. Beneke, R.F. Sandenbergh, Corrosion Science 29 (1989) 543.
[16] V. Ciahl, Corrosion Science 20 (1984) 737.
[17] A.O. Majidi, M.A. Streicher, Corrosion Science 24 (1984) 393.
[18] Yamamoto, S. Takahashi, Proceedings of the Symposium in Molten Carbonate Fuel Cell Technology, in: J.R. Selman, T.D. Claar (Eds.), The Electrochemical Society, Pennington, NJ, 1984, p. 181.
[19] A Development of 2 kW Molten Carbonate Fuel Cell Stack Technical report, TR.93T-J03.97.01, Korea Electric Power Research Institute, 1997, p. 387.
[20] S. Ramamurthy, A. Atrens, I.O. Smith, Materials Science Forum, Vols. 44 and 45, Copyright Trans Tech Publications, Switzerland, 1988, p. 139.
[21] K. Osozawa, H.J. Engell, Corrosion Science 6 (1966) 389.
[22] K. Osozawa, K. Bohnenkamp, H.J. Engell, Corrosion Science 6 (1966) 421.
[23] R.G. Faulkner, J. Material Science 16 (1981) 373.
[24] R.N. Iyer, H.W. Pickering, Environmental Degradation of Engineering Materials Conference, State College, Pennsylvania, 1987.
[25] B.W. Bennett, Pickering, Acta Metall. 36 (1988) 539.
[26] B.W. Bennett, Pickering, Metallurgical Transactions A 18A (1987) 1117.
[27] K. Cho, M.I. Abdulsalam, H.W. Pickering, J. Electrochem. Soc. 145 (1998) 1862.
[28] H.S. Hsu, J.H. DeVan, M. Howell, J. Electrochem. Soc. 134 (1987) 2146.
[29] H.S. Hsu, J.H. DeVan, J. Electrochem. Soc. 134 (1987) 3038.